Marine Structures 53 (2017) 124–135

Contents lists available at ScienceDirect

Marine Structures

journal homepage: www.elsevier.com/locate/marstruc

Scaling of lateral pile *p-y* response in clay from laboratory stress-strain curves

Youhu Zhang [a, *], Knut H. Andersen [b]

[a] Technical Lead Offshore Geotechnics, Norwegian Geotechnical Institute, Sognsveien 72, 0855 Oslo, Norway
[b] Norwegian Geotechnical Institute, Sognsveien 72, 0855 Oslo, Norway

ARTICLE INFO

Article history:
Received 9 October 2016
Accepted 6 February 2017
Available online 17 February 2017

Keywords:
Pile
Clay
Lateral loading
p-y spring
Stress-strain

ABSTRACT

This paper deals with the static lateral load-displacement response (*p-y* spring) of a pile slice in soil. The response is governed by a localised flow-around soil failure mechanism. A model is proposed that allows for construction of site-specific *p-y* springs by directly scaling the soil stress-strain response measured in laboratory tests. This model is based on an extensive parametric finite element study and can explicitly account for the effect of pile-soil interface roughness factor on both the strength and shape of the *p-y* spring. The model demonstrates excellent agreement with the *p-y* responses calculated numerically. An example application illustrates the capability of the model to predict the overall pile response by comparison with full three dimensional finite element analysis. The proposed model is compared with existing models in the literature, where similarities and differences are discussed and highlighted. The model provides practising engineers with a simple yet powerful approach to use site-specific *p-y* curves in design based on element soil behaviour measured in laboratory, without the need for advanced numerical analyses.

1. Introduction

Piles, especially offshore piles, often have to be designed to resist lateral loading. The load-transfer approach is usually adopted for pile design, in which soil resistance is represented by lateral load (p, defined as force per unit pile length) versus displacement (y) springs along the pile and the overall pile response is solved by a beam-column approach. It is well known that for a laterally loaded slender pile in clay, two soil failure mechanisms may exist. In the upper part, soil fails in a conical wedge that extends to the soil surface. A gap may also form along the interface between the pile and the soil on the active side if the suction between the pile and the soil is lost. At a certain depth, however, the soil failure mechanism transits into a localised plane flow-around mechanism, as the soil resistance encountered in this mechanism becomes less than failure in conical wedge. Randolph and Houlsby [1] studied the limiting lateral bearing pressure (i.e. peak of the *p-y* spring) for a circular cylinder failing the soil in a plane strain flow-around mechanism based on plasticity theory. The *p-y* spring that leads up to the peak for the same mechanism is subject of this study. The *p-y* springs appropriate for shallow wedge failure, gapping, and the local behaviour at the tip are beyond the scope of this paper.

* Corresponding author.
E-mail addresses: youhu.zhang@ngi.no (Y. Zhang), knut.h.andersen@ngi.no (K.H. Andersen).

http://dx.doi.org/10.1016/j.marstruc.2017.02.002
0951-8339/

1.1. Literature review

In the offshore industry, the API guideline, latest version as [2], is conventionally used to design the pile foundations. The static p-y spring model in clay recommended in API originates from the field pile tests performed at Sabine River in the 1950s and reported in Matlock [3]. The static p-y model relates the mobilised lateral resistance to the normalised lateral displacement in a power law relation:

$$\frac{p}{p_u} = 0.5\left(\frac{y}{y_c}\right)^{0.33} \leq 1 \tag{1}$$

where p_u = the ultimate lateral resistance (force) per unit pile length; y = lateral displacement; $y_c = 2.5 \cdot \varepsilon_{50} \cdot D$, with ε_{50} defined as axial strain at which 50% of maximum deviator stress is mobilised in an undrained compression test (the API document is not specific on the type of tests. In practice, this is often chosen from unconsolidated undrained (UU) compression tests). D = pile diameter.

Full mobilisation of the API p-y spring is achieved (i.e. $p/p_u = 1$) at $y = 8y_c$. It must be recognised that the Matlock p-y model has been developed and calibrated mainly against the field tests performed lightly over-consolidated clays at the Sabine River. The applicability of the empirical model to other soil conditions should therefore be checked.

Based on centrifuge tests detailed in Jeanjean [4] and finite element analyses detailed in Templeton [5], the following expression, denoted as Jeanjean p-y model in this paper, is proposed in Jeanjean [4]:

$$\frac{p}{p_u} = \tanh\left(\frac{G_{max}}{100 s_u}\left(\frac{y}{D}\right)^{0.5}\right) \tag{2}$$

where G_{max}/s_u = initial shear modulus (G_{max}) over shear strength (s_u) ratio;

The remaining parameters are as defined previously.

Eq. (2) includes the influence of the G_{max}/s_u ratio on the shape of the p-y spring. However, it is reasonable to anticipate that not only the initial stiffness of the soil, but also the stress-strain response beyond the initial phase will influence the p-y response of the pile. It should be noted that the Jeanjean p-y model is calibrated against testing/finite element analyses in Kaolin soil with a specific stress-strain behaviour. This perhaps explains why only G_{max}/s_u is formulated in the model. Furthermore, the proposed impact of G_{max}/s_u on the pile p-y response is not verified through either model tests or numerical analyses, but is rather based on postulation.

It should be further noted that Eq. (1) and Eq. (2) imply infinite stiffness at $y = 0$. In practice, a limitation of $(p/p_u)/(y/D) \leq x \cdot (G_{max}/s_u)$ is applied, with x typically taken in the range 0.35–0.5. This ensures an initial stiffness that is consistent with elastic solutions.

Bransby [6] reported a finite element study of a plane strain pile slice in nonlinear elastic soils with power law stress-strain relation expressed as $\tau = a\gamma^b$ where a and b are material constants. It is demonstrated that the resulting p-y curve from the finite element analysis can be scaled from the stress-strain curve by a scaling coefficient that varies with the power law factor b. The significance of the work is that it illustrates the self-similarity between the soil stress-strain response and the resulting p-y response of a translating pile slice.

Osman and Bolton [7] demonstrated that it is possible to scale the soil stress-strain response to the load-settlement response of a circular foundation vertically loaded on undrained clay through the so-called moblisable strength design (MSD) concept. Similar concepts are applied to study the lateral load transfer response of a pile slice deforming in plane strain mode by Klar [8], Klar and Osman [9] and recently by Yu et al. [10]. Load transfer (p-y) curves can be derived by solving energy dissipation equations over a pre-defined pattern function (failure mechanism). The method is shown to provide comparable p-y curves to those calculated by finite element analyses. Klar and Randolph [11] also applied the MSD concept to study the pile head load displacement response.

1.2. Motivation of this study

The work by Bransby [6], Klar [8], Klar and Osman [9] and Yu et al. [10] demonstrates from the numerical and theoretical perspectives that it is possible and rationale to link the pile p-y curves to the soil stress-strain response. Erbrich et al. [12] present a procedure that calculates site-specific envelope p-y curves by means of finite element/finite difference analyses using the stress-strain responses measured in laboratory tests and subsequently uses them in assessment of pile response under cyclic loading. With computation power of modern computers and availability of advanced soil model that can follow the soil non-linear stress-strain response, finite element parametric analyses of p-y response of a pile slice can be easily performed, with sufficient discretisation accuracy. The soil flow mechanism is automatically calculated in a finite element analysis and the p-y curve is a direct analysis output. In this study, a large parametric study of a pile slice p-y response over a wide range of soil stress-strain behaviour and pile-soil interface roughness are performed. The motivation of the analyses is to come up with a simple p-y model that allows for construction of site-specific p-y curves from fundamental soil stress-strain response measured in the laboratory, without the need of advanced numerical analyses.

2. Methodology and finite element model

A horizontal slice of a slender pile is analysed in Plaxis 3D [13]. The slice is 1 m in thickness, representing a 1 m pile segment of a long pile. Vertical movement on the top and bottom boundaries of the model is constrained, therefore enforcing a plane strain condition. The *p-y* springs derived from such analyses are therefore only relevant for the part of a pile where localised flow-around mechanism is governing. Methods to predict the onset depth of localised flow-around mechanism can be found, for example, in Murff and Hamilton [14], Yu et al. [15] and Zhang et al. [16].

Fig. 1 shows the finite element model. Due to symmetry, only a half-pile segment is modelled. The lateral extent of the boundaries is selected to 10 times pile diameters (D) from the centre of the pile. Note that in an idealised elastic material, the elastic *p-y* stiffness is dependent on the lateral extent of the boundary, as demonstrated by Baguelin et al. [17]. In the current study, nonlinear soil response is considered and the lateral boundary is chosen such that the boundary effect is negligible. The lateral force is applied as a distributed pressure on the vertical symmetry face of the pile, which is modelled as a rigid body. The pile is loaded until the load-displacement curve becomes flat, indicating ultimate state.

Small strain finite element analyses are performed, and the geometric nonlinearity is not considered. The soil-pile interface is simulated by interface elements in Plaxis. Separation between the soil-pile interfaces is not allowed. The tangential property is controlled by the specified interface strength, and relative slip between the pile-soil interface can occur if the mobilised shear stress on the interface reaches the specified limit.

It should be noted that the boundary condition adopted in the finite element model ignores the shear stress that may be developed on the top and bottom of the pile slices. The current model therefore does not capture the complex three dimensional pile-soil interaction fully. Rather the model considered here is a simplification of the problem. The impact of the simplification will be examined when the *p-y* curves developed from the current finite element analyses are used to predict the overall pile response.

The finite element mesh has been benchmarked against the theoretical solutions for the limiting bearing pressure of circular cylinder that fails the soil in plane strain flow-around mechanism presented by Randolph and Houlsby [1]. For a rough pile-soil interface, the numerical model calculates a limiting bearing pressure of $12.52s_u$, as compared to the theoretical value of $11.94s_u$. This represents a numerical overshoot of 4.9% due to discretisation error. A mesh sensitivity study has been performed and demonstrates that when the calculated *p-y* response is normalised by the calculated ultimate bearing pressure and pile diameter (which gives the shape of the *p-y* curve), the effect of numerical over-shooting is negligible.

3. Soil model and parametric range

Due to the plane strain condition (no vertical soil movement), the consolidation stresses and the soil stress-strain behaviour in a triaxial test are not directly relevant for determining the shape and strength of the *p-y* spring. The deformation characteristics of the pile slice is better represented by the shearing in the direct simple shear mode (s_u^{DSS}), although the plane of shearing is vertical instead of horizontal as is the case in conventional direct simple shear tests. In practice, this is normally not differentiated. Bjerrum [18] offers comparisons of DSS tests performed in vertical and horizontal planes, and the difference between the two seems to vary with soil plasticity.

The soil is described by the NGI-ADP model [19]. The model is a total stress soil model for simulating undrained anisotropic behaviour of clay. It follows a Tresca type yield criterion, and interpolates between s_u^{DSS}, s_u^C (shear strength in triaxial compression) and s_u^E (shear strength in triaxial extension) for shearing in directions not covered by s_u^{DSS}, s_u^C and s_u^E. The model features a non-linear hardening law that links the current yield stress with the current plastic shear strain. The hardening law parameters can be calibrated against site-specific stress-strain response measured in soil laboratory tests. The model is therefore suitable for both undrained ultimate capacity and deformation analyses. The model is available in the commercial

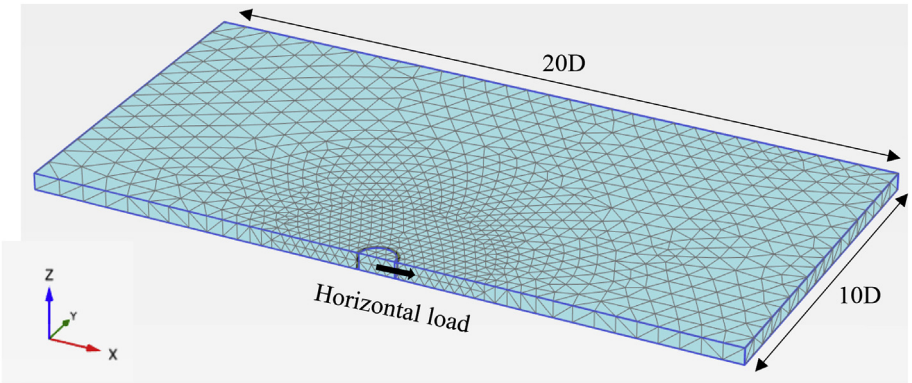

Fig. 1. Illustration of the finite element model.

finite element package Plaxis 3D as a built-in soil model. For the current problem, stress-strain response and ultimate shear strength in triaxial compression and triaxial extension modes are not relevant, and only those in DSS mode are considered.

In the NGI-ADP model, the following plastic hardening rule is assumed:

$$\frac{\tau}{s_u} = 2\frac{\sqrt{\gamma^p \Big/ \gamma_f^p}}{1+\gamma^p \Big/ \gamma_f^p} \tag{3}$$

whereτ = currently mobilised shear stress ; s_u = the shear strength of soil (DSS strength in this case); γ^p = the current plastic shear strain; $\gamma^p{}_f$ = the plastic shear strain at failure (full mobilisation).

The total shear strain γ associated with the currently mobilised shear stress τ is the summation of elastic and plastic shear strain components (γ^e and γ^p respectively):

$$\gamma^t = \gamma^e + \gamma^p = \frac{\tau}{G_{max}} + \gamma^p = \frac{\tau/s_u}{G_{max}/s_u} + \gamma^p \tag{4}$$

where G_{max}/s_u is the small strain shear modulus over shear strength ratio and is assumed constant throughout.

In the stress-strain relation described by Eqs. (3) and (4), the G_{max}/s_u ratio and the plastic failure strain $\gamma^p{}_f$ can be calibrated against site-specific data so that the actual soil response is simulated in the numerical model. This is illustrated in Fig. 2 where the stress-strain responses of three marine clays are described by the NGI-ADP model. The model parameters shown on the figure were found by curve-fitting that give best fit to the lab results, with the choice of G_{max}/ s_u ratio guided by the empirical correlations between G_{max}/s_u, over-consolidation ratios (OCR) and plasticity index (I_p) proposed by Andersen [20]. Fig. 2(a) presents the stress-strain responses measured on undisturbed Drammen clay (plasticity index I_p = 27%) consolidated to three different OCR values [20]. Fig. 2(b) presents the stress-strain responses measured on undisturbed Onsøy clay at two different depths [21]. The Onsøy clay is a normally consolidated marine clay, with an apparent OCR of about 1.4 and an average I_p of 33%. Fig. 2(c) presents the stress-strain responses measured at different depths on normally consolidated high plasticity (I_p averages around 50%) Gulf of Mexico (GoM) clay at the Marlin site [22]. It is illustrated that the normalised GoM stress-strain curves at different depths plot closely on top of each other, which is also exhibited by the Onsøy clay. The examples presented here demonstrate that the hardening relationship adopted by the NGI-ADP model is indeed well-suited for describing the stress-strain behaviour of clays.

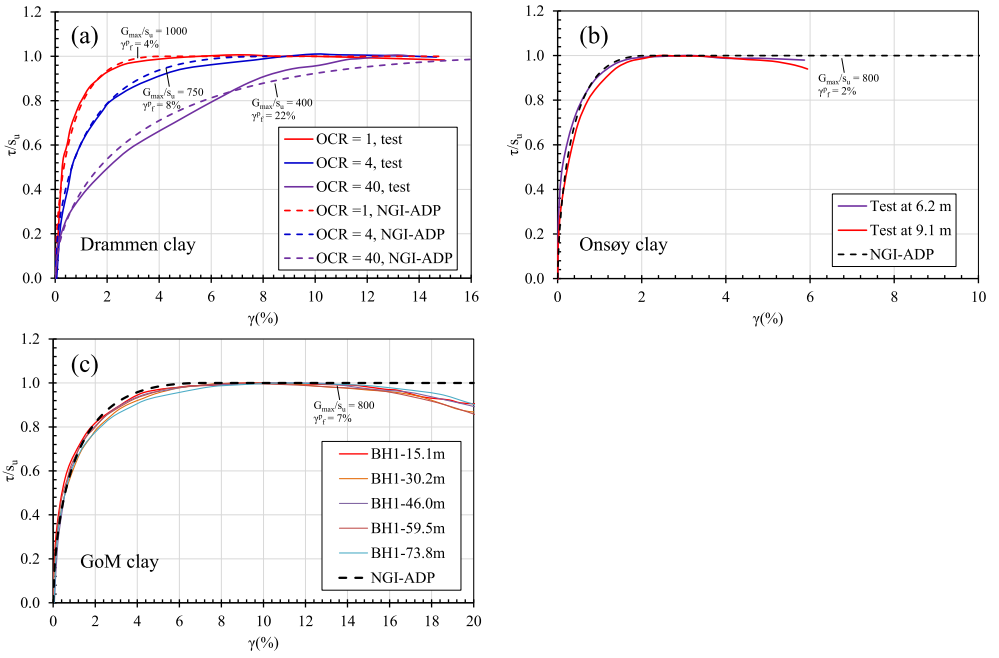

Fig. 2. Stress-strain responses measured in DSS tests for three clays and descriptions with NGI-ADP model (test data digitised from Andersen [20], Lunne et al. [21] and Jeanjean et al. [22]).

In the current study, parametric finite element analyses using the pile slice model over a wide range of soil stress-strain responses are performed. The corresponding *p-y* springs are obtained from these analyses. The following stress-strain ranges are considered in the parametric study.

G_{max}/s_u: 100, 250, 500, 1000, 5000

γ_f^p (%): 2, 4, 6, 8, 10, 12, 16, 20

In addition, the parametric study also includes the effect of pile-soil interface roughness (α) on the resulting *p-y* springs. The interface roughness factor α is defined as ratio of available interface shear strength to the intact strength of the adjacent soil. Roughness factor $\alpha = 0$, 0.5, 0.75 and 1 are considered.

Fig. 3 illustrates an example of the stress-strain curves constructed for different plastic failure strains with $G_{max}/s_u = 250$ according to Eqs. (3) and (4).

4. Results and proposed p-y model

4.1. Numerically calculated p-y springs

The results from the analyses are series of *p-y* springs. For each suite of stress-strain responses corresponding to a specific G_{max}/s_u ratio, a *p-y* spring is calculated for each pertinent combination of interface roughness and plastic failure strain. In total, 140 analyses were performed, producing 140 *p-y* springs. Fig. 4 shows the *p-y* springs calculated for a rough (i.e. $\alpha = 1$) pile-soil interface and stress-strain responses shown in Fig. 3.

From Fig. 4, it can be seen that the shape of the *p-y* springs bear strong similarities with the soil stress-strain curves that were used as input to derive them. This is as observed by other researchers [6,9,23]. The stiffer the soil stress-strain response, the stiffer is the calculated *p-y* response, and vice versa. It is therefore interesting to explore the possibility of "scaling" the stress-strain response to the *p-y* response, which is attempted below.

4.2. Proposed p-y model

The idea of scaling the stress-strain curve to the *p-y* curve is illustrated in Fig. 5. A point on the stress-strain curve with mobilisation in shear stress (τ/s_u) corresponds to a point on the *p-y* curve with the same level of mobilisation in lateral bearing pressure ($p/p_u = \tau/s_u$). The corresponding normalised lateral displacement (y/D) can be scaled from the shear strain with two scaling coefficients, ξ_1 and ξ_2, which apply to the elastic and plastic components of the shear strain respectively. The elastic and plastic shear strains are determined from Eq. (3) and Eq. (4).

Both scaling coefficients ξ_1 and ξ_2 are found to be dependent on the interface roughness factor α. For simplicity, a constant $\xi_1 = 2.8$ and a ξ_2 that varies linearly with α is found to give a satisfactorily good fit to the numerical results.

$$\xi_2 = 1.35 + 0.25\alpha \tag{5}$$

The ultimate lateral resistance per unit pile length p_u, calculated as $N_p \cdot s_u \cdot D$ where N_p is the ultimate bearing capacity factor, is also related to the interface roughness factor by

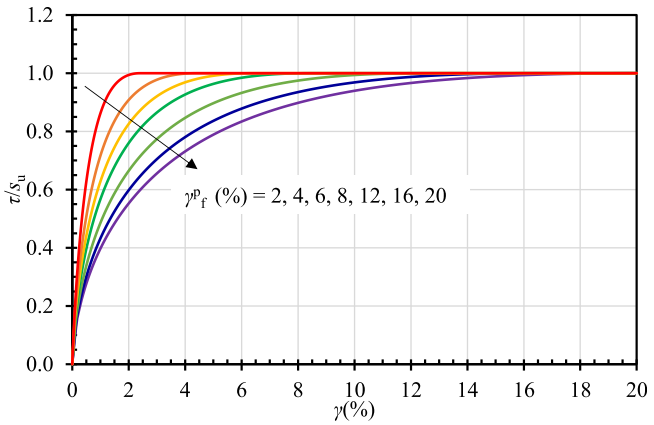

Fig. 3. Example stress-strain response ($G_{max}/s_u = 250$).

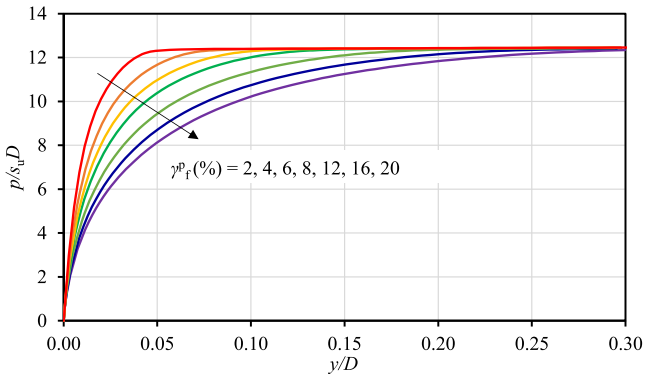

Fig. 4. Example *p-y* springs from pile slice analyses ($G_{max}/s_u = 250$, $\alpha = 1$).

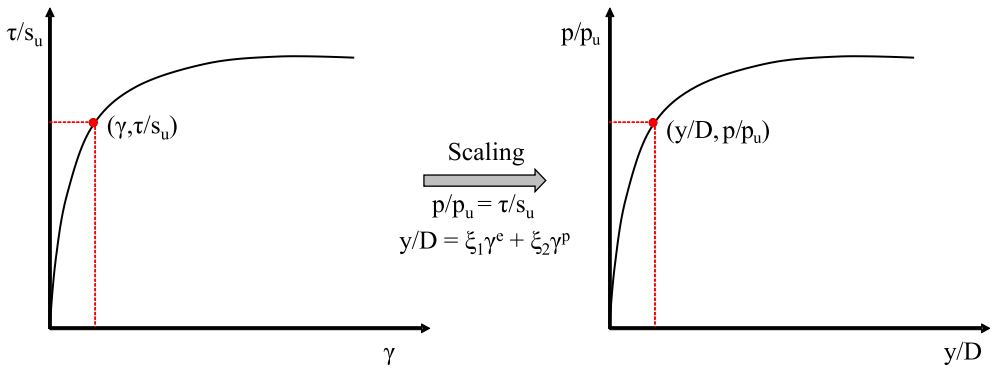

Fig. 5. Schematic illustration of proposed *p-y* model.

$$N_p = 9 + 3\alpha \tag{6}$$

The relation in Eq. (6) is based on results presented by Randolph and Houlsby [1], as illustrated in Fig. 6. The current analyses reveal the same trend, though numerically, the N_p values are over-estimated by 5–7% compared to the theoretical values.

The inclusion of the roughness into the *p-y* model allows for site-specific assessment of interface roughness according to soil conditions and set-up effects and eventual application in lateral pile capacity design, in the same way as axial capacity design. Furthermore, in the current design practice, axial and lateral loading capacities are often verified separately, without

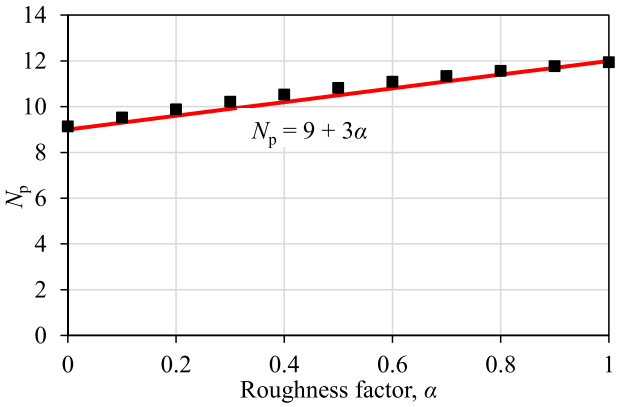

Fig. 6. Variation of N_p with interface roughness (results after Randolph and Houlsby 1984).

accounting for the interaction between the two. An indirect way to partially account for the interaction is to consider the axial skin friction utilisation and reduce the available interface roughness accordingly when verifying the lateral resistance [16,24]. The current model provides the possibility to specifically account for interface roughness, and/or to account for the influence of axial loading.

Fig. 7 illustrates an example where *p-y* springs constructed by the proposed model are compared with those calculated numerically (the constructed *p-y* springs are shown in dashed lines). An excellent match is demonstrated. Similarly, a good match is also obtained for other roughness factor and G_{max}/s_u combinations, and is thus not shown. Note that in this demonstration, the numerically calculated N_p factor is used when applying the proposed *p-y* model, to avoid distortions.

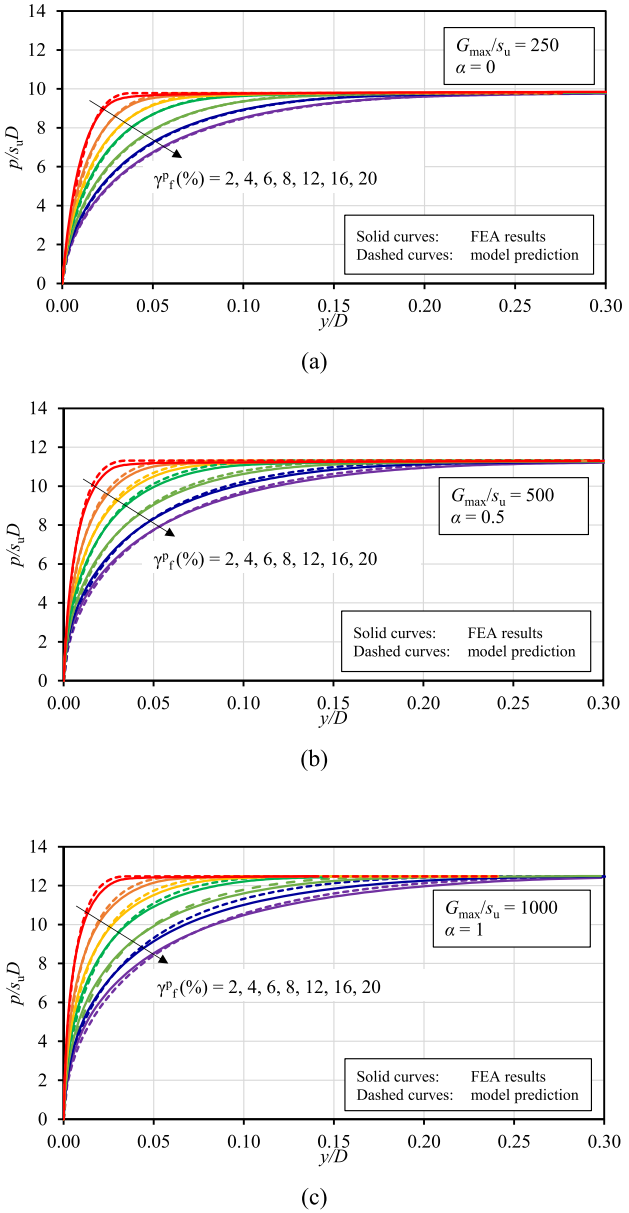

Fig. 7. Comparison of retrospectively calculated *p-y* springs against numerical results: (a) $G_{max}/s_u = 250$, $\alpha = 0$; (b) $G_{max}/s_u = 500$, $\alpha = 0.5$; (c) $G_{max}/s_u = 1000$, $\alpha = 1$.

5. Discussions

5.1. Elastic scaling coefficient

Theoretical solutions for the load transfer response in elastic material suggest a gradient $k_{py} = p/y \approx 4G_{max}$ [17,25]. With a best-fit $\xi_1 = 2.8$, and $p_u/s_u D = 9$ and 12 for a smooth and a rough interface respectively, the model implies an elastic gradient $k_{py} = 3.2$ to $4.3G_{max}$ for smooth and rough interface respectively when the plastic strain is neglected. This demonstrates that the ξ_1 value, obtained by curve-fitting, does offer a reasonable agreement with the theoretical value.

5.2. Comparison with Matlock [3]

In the Matlock model, referring to Eq. (1), the lateral resistance mobilisation is expressed as a power law relation to the normalised lateral displacement. The displacement used for normalisation is y_c, defined as lateral displacement at 50% mobilisation, and can be calculated as $2.5 \cdot \varepsilon_{50} \cdot D$. In terms of shear strain, this is in a UU test equivalent to $y_c = 2.5 \cdot (2/3 \cdot \gamma_{50}) \cdot D = 1.67 \cdot \gamma_{50} \cdot D$, where γ_{50} is the shear strain corresponding to ε_{50} (in an undrained triaxial test, the relationship between radial and axial strain is $\varepsilon_r = -\varepsilon_a/2$ due to zero volumetric strain. Therefore, shear strain $\gamma = \varepsilon_a - \varepsilon_r = 3/2\ \varepsilon_a$. Correspondingly, $\gamma_{50} = 3/2 \cdot \varepsilon_{50}$). In relation to the current model, assuming the "elastic" displacement component (similarly the elastic shear strain) is negligible, the equivalent y_c can be calculated as $y_c = \xi_2 \cdot \gamma_{50} \cdot D$. The current model suggests $\xi_2 = 1.35 + 0.25\alpha$. With a fully rough interface, $\xi_2 = 1.6$, which is very close to 1.67 as implied by the Matlock p-y model.

It is noticed that the Matlock p-y expression, i.e. Eq. (1), is similar to the strength mobilisation framework proposed by Vardanega and Bolton [26] for clay, which they argue that for most clays, the stress-strain response in shearing in the moderate stress range can be expressed reasonably by a power law:

$$\frac{\tau}{s_u} = 0.5\left(\frac{\gamma}{\gamma_{M=2}}\right)^b \text{ for } 0.2 \le \tau/s_u \le 0.8 \tag{9}$$

where $\gamma_{M=2}$ is the so-called mobilisation strain, which refers to shear strain at 50% strength mobilisation. Therefore, $\gamma_{M=2} = \gamma_{50}$. Parameter b is a material constant and is within a range of 0.3–1.2 with a mean value of 0.6. Vardanega et al. [27] further found that $\gamma_{M=2}$ value increases with OCR for Kaolin clay, which leads to increasingly more ductile response. The data for Kaolin clay also suggests a slight increase of b value with OCR.

Essentially, the Matlock p-y model can be understood as a similar model to the currently proposed model that scales the soil stress-strain response to the p-y response, although the exact format of expression used to describe the soil stress-strain responses is different. The scaling coefficient, embedded in the definition of y_c for the Matlock model is even found to be similar to the current model for a rough pile-soil interface, as discussed previously. However, the Matlock model implies a constant b value of 0.33 for the power law description of the soil stress-strain response, which is probably appropriate for the Sabine River slightly over-consolidated clay on which the model was calibrated against. However, for other clays, when a different b value is required to provide a reasonable fit to the soil stress-strain response, the Matlock p-y model could result in inappropriate p-y curves.

It should be further noticed that in the Matlock model (as well as in API), a limiting N_p factor of 9 is recommended. This corresponds to the theoretical value obtained for fully smooth pile-soil interface and can lead to underestimation of pile capacity.

5.3. Comparison with Jeanjean p-y model

Fig. 8(a) illustrates the soil stress-strain response measured in a laboratory static DSS test in Kaolin clay considered in Templeton [5], against which Templeton's finite element model is calibrated. The soil response is curve-fitted by the NGI-ADP

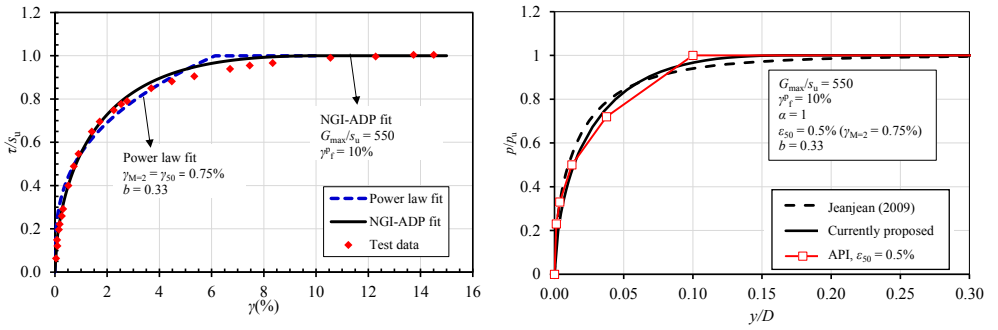

Fig. 8. Comparison of p-y springs in normalised form.

soil model with the best-fit parameters $G_{max}/s_u = 550$ and $\gamma^p_f = 10\%$, as well as by the power law relation with $\gamma_{M=2} = \gamma_{50} = 0.75\%$ (equivalently $\varepsilon_{50} = 0.5\%$) and $b = 0.33$ (as implied by Matlock model), as shown in Fig. 8(a). It can be seen that, with the respective set of parameters, both the NGI-ADP model and the power law relation provide reasonable fits to the experimental stress-strain response. Fig. 8(b) compares the p-y springs in the normalised form ($y/D - p/p_u$) calculated by the currently proposed model, with the Jeanjean model, as well as the API model (simplified format of Matlock model).

It can be seen that a reasonably good agreement is obtained between p-y springs calculated by the Jeanjean model and the currently proposed model. This confirms the consistency between two independent numerical studies when the same set of input parameters are considered. However, in the Jeanjean model, the G_{max}/s_u value is the only parameter that controls the shape of the p-y springs; and furthermore, the proposed trend of p-y springs with G_{max}/ s_u ratio is not based on parametric studies, but based on mere postulation. The current model, based on a parametric study over a wide range of soil responses in shearing, therefore allows for explicit consideration of the full stress-strain response from small strain to large strain at failure on the p-y springs through parameters of G_{max}/s_u and γ^p_f

Fig. 8(b) also illustrates that the API p-y model, based on Matlock [3], does provide a reasonable good match to the currently proposed model in the normalised format ($p/p_u - y/D$) for the case considered here. This is as expected since the power law expression with $b = 0.33$ does provide a good description of the soil stress-strain behaviour. However, the suitability of the API p-y model will become questionable when the power law expression with $b = 0.33$ cannot accurately describe the soil stress-strain response in other soil conditions, for example in over-consolidated clays. It should also be borne in mind that the API p-y model adopts a limiting N_p factor of 9, regardless of interface roughness. This, in most cases, underestimate the capacity.

5.4. On generality of the proposed p-y model

In this study, the soil stress-strain response is described by the NGI-ADP model with the hardening described by the mathematical format of Eqs. (3) and (4). In principle, the scaling relationship between the stress-strain response and the p-y response should be general to the soil model adopted for the analyses. Other forms of mathematical formulations which describe the soil response sufficiently, should lead to similar conclusions. In order to demonstrate this, additional p-y analyses were performed in the finite element package Abaqus 6.14–1 [28]. A finite element model, similar to the Plaxis model described in Section 2, was developed. A Tresca failure criterion was followed. The pre-failure stress-strain response was specified in a table format, which is not limited to any specific mathematical format. For simplicity, a fully rough interface was considered.

Fig. 9 presents a series of finite element analyses with four different stress-strain responses. As expected, the resulting p-y responses show strong similarity to the soil stress-strain inputs. The p-y model proposed in Section 4.2 is applied to back-predict the p-y responses by taking $\gamma^e = \tau/G_{10}$, $\gamma^p = \gamma - \gamma^e$, where G_{10} is the secant shear modulus at 10% shear stress mobilisation and can be calculated from the stress-strain curve given. It is found that a slightly smaller $\xi_1 = 2.6$ gives better results than $\xi_1 = 2.8$, while using the same ξ_2 value. A reasonably good agreement between the model predictions and FEA results is demonstrated. It is noted that for the two curves to the right, the model predicts slightly stiffer responses than FEA at high mobilisation levels. This is related to the shape of the stress-strain curve. It is observed by the authors that as the curvature of the stress-strain curve reduces, the difference between the p-y model and the FEA prediction increases at high mobilisation levels. For the extreme case of a linearly elastic perfectly plastic stress-strain response, Fig. 10 illustrates that the p-y model is capable of predicting the response well up to $p/p_u = 0.6$. For higher mobilisation levels, the calculated p-y response by FEA is softer than the model prediction. Although the material response is linearly elastic perfectly plastic, the p-y response exhibits non-linearly as some soil elements reach yield state earlier than the others. It should be stressed that natural soil response is rarely linearly elastic perfectly plastic. The proposed p-y model is therefore believed of general applicability for soils.

The finite element results calculated using the NGI-ADP soil model are also re-interpreted, and it is demonstrated that by taking $\gamma^e = \tau/G_{10}$, $\gamma^p = \gamma - \gamma^e$, $\xi_1 = 2.6$ and $\xi_2 = 1.35 + 0.25\alpha$, the proposed model predicts excellently the p-y responses

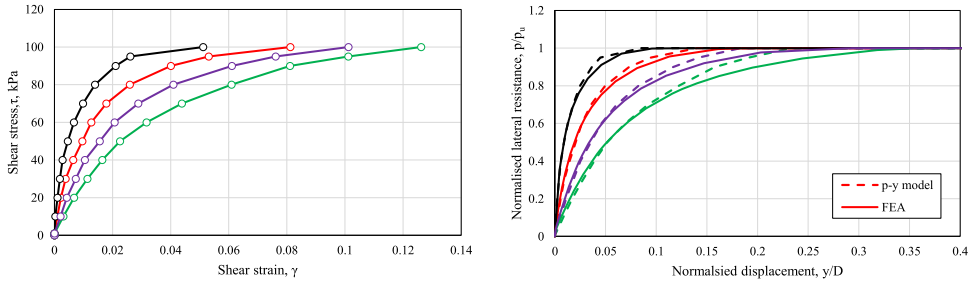

Fig. 9. Stress-strain inputs and corresponding p-y output.

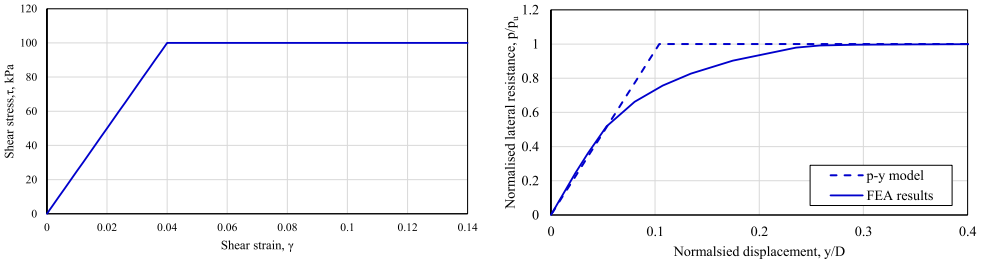

Fig. 10. Comparison of model prediction and finite element result for a linearly elastic perfectly plastic stress-strain response.

calculated by the finite element analyses. The significance of this finding is that one does not need to go through the intermediate procedure of finding the curve fitting parameters G_{max}/s_u and γ_f^p for the NGI-ADP model or any other mathematical model in order to apply the proposed *p-y* model. The measured stress-strain relationship can be applied directly to derive the site-specific *p-y* response. One may argue that G_{max} is a better parameter than G_{10} as G_{max} is measured directly in the laboratory and is usually available for design. However, in the case when G_{max} measurement is not available and the stress-strain curve is the only information available, one may evaluate G_{10} from the stress-strain response and apply the model by taking $\gamma^e = \tau/G_{10}$, $\gamma^p = \gamma - \gamma^e$ and $\xi_1 = 2.6$, $\xi_2 = 1.35 + 0.25\alpha$. When G_{max} is available, the model should be applied by taking $\gamma^e = \tau/G_{max}$, $\gamma^p = \gamma - \gamma^e$ and $\xi_1 = 2.8$, $\xi_2 = 1.35 + 0.25\alpha$.

6. Example application

In order to demonstrate the usefulness of the proposed *p-y* curves, a typical offshore driven pile in a normally consolidated clay profile is analysed by three dimensional finite element analyses (FEA) in Plaxis 3D and by a simplified beam-column analysis, using the *p-y* springs constructed from the currently proposed model. The pile is 84" (2.134 m) in diameter, 0.06 m in wall thickness, and penetrated 40 m at pile tip. The strength profile is: $s_u^{DSS} = 5.1 + 2.4z$, where z is the depth below seafloor. The soil is modelled by the NGI-ADP model in Plaxis, with the relevant parameters in DSS shearing being: $G_{max}/s_u^{DSS} = 500$, and $\gamma^p{}_f = 4\%$. An interface roughness factor $\alpha = 1$ is considered (i.e. fully rough). The pile material is modelled as linearly elastic, with a Young's modulus of 210 GPa. Tension crack is not allowed in the finite element analysis, meaning that suction is assumed.

Fig. 11 presents a comparison of the predicted pile response under a pile head lateral load of 6900 kN by the three dimensional finite element analysis and by the simplified beam-column analysis using *p-y* springs. Note that in the finite element analysis, a shallow wedge failure is observed in the upper approximately two pile diameters below the soil surface. In the beam-column analysis, the *p-y* springs corresponding to flow-around failure is used along the entire pile length, although a reduced lateral bearing capacity factor (N_p) is used in the shallow wedge part, following the recommendation by Zhang et al. [16]. Fig. 11 demonstrates an excellent match in the predicted pile responses between the *p-y* springs and the full three dimensional finite element simulation, both in terms of pile displacement and structural forces.

The reason for the good match is further examined in Fig. 12, where the mobilised *p-y* reaction in the finite element analysis is compared with the *p-y* curves constructed according to the currently proposed model. A close match is demonstrated, confirming the validity of the proposed *p-y* model.

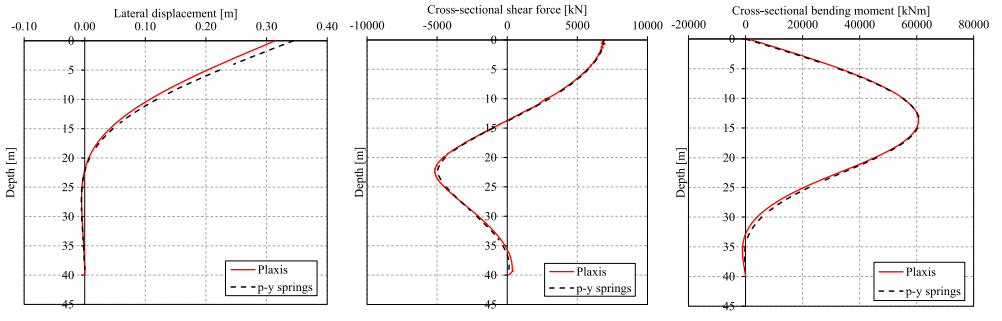

Fig. 11. Comparison between finite element analysis and simplified beam-column analysis.

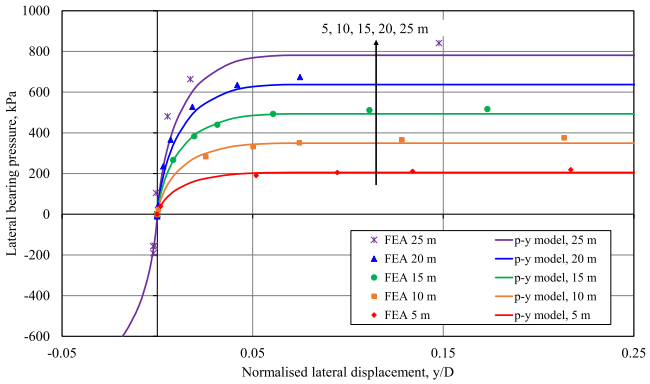

Fig. 12. Comparison of mobilised *p-y* response calculated in full three dimensional finite element analysis against proposed *p-y* model.

7. Conclusions

Assuming a plane strain condition, the lateral *p-y* response of a pile slice is examined by means of finite element analyses over a wide parametric range of soil stress-strain behaviour. Based on the results, a new model that enables construction of *p-y* springs by simply scaling the soil stress-strain response measured in laboratory DSS test is proposed. One of the two scaling coefficients is a constant and the other is a simple function of the pile-soil interface roughness factor. It is demonstrated that the *p-y* model is not tied to a specific mathematical format used for description of the soil stress-strain response. An example application demonstrates excellent capability of the model to predict the overall pile response which is confirmed by comparison with full three dimensional finite element analysis.

The model is suited for the deeper part of the pile where localised flow-around mechanism is governing the failure in lateral loading. The model provides practising engineers with a simple yet powerful approach to use site-specific *p-y* curves in design based on element soil behaviour measured in laboratory, without the need for advanced numerical analyses. Furthermore, the influence of interface roughness factor can be explicitly considered, through both the ultimate capacity and the shape of the *p-y* spring.

Acknowledgements

The authors wish to gratefully acknowledge the financial support received through a NGI internal research project, which is partially funded by the Norwegian Research Council. Discussions and feedbacks from NGI colleagues Dr Hans Petter Jostad, Dr Rasmus Tofte Klinkvort, Dr Noel Boylan and Dr Andrew Deeks are gratefully appreciated. The authors also wish to thank Prof Malcolm Bolton for reading and commenting on the manuscript, which inspired some of the discussions presented in this paper.

References

[1] Randolph MF, Houlsby GT. The limiting pressure on a circular pile loaded laterally in cohesive soil. Geotechnique 1984;34:613–23.
[2] API. Geotechnical and foundation design considerations. ANSI/API Recommended Practice 2GEO Addendum 2014;1.
[3] Matlock H. Correlations for design of laterally loaded piles in soft clay. In: Offshore technology conference. Houston: Texas; 1970. p. OTC 1204.
[4] Jeanjean P. Re-assessment of p-y curves for soft clays from centrifuge testing and fintie element modeling. In: Offshore technology conference. Houston: Texas; 2009. p. OTC 20158.
[5] Templeton JS. Finite element analysis of conductor/seafloor interaction. In: Offshore technology conference. Huston: Texas; 2009. p. OTC 20197.
[6] Bransby MF. Selection of p-y curves for the design of single laterally loaded piles. Int J Numer Anal Methods Geomech 1999;23:1909–26.
[7] Osman AS, Bolton MD. Simple plasticity-based prediction of the undrained settlement of shallow circular foundations on clay. Geotechnique 2005;55:435–47.
[8] Klar A. Upper bound for cylinder movement using "elastic" fields and its possible application to pile deformation analysis. Int J Geomech 2008;8:162–7.
[9] Klar A, Osman AS. Load-displacement solutions for piles and shallow foundations based on deformation fields and energy conservation. Geotechnique 2008;58:581–9.
[10] Yu J, Huang M, Li S, Leung CF. Load-displacement and upper-bound solutions of a loaded laterally pile in clay based on a total-displacement-loading EMSD method. Comput Geotech 2017;83:64–76.
[11] Klar A, Randolph MF. Upper-bound and load-displacement solutions for laterally loaded piles in clays based on energy minimisation. Geotechnique 2008;58:815–20.
[12] Erbrich CT, O'Neill MP, Clancy P, Randolph MF. Axial and lateral pile design in carbonate soils. Perth, Australia. In: Gourvenec S, White D, editors. 2nd international symposium on frontiers in offshore geotechnics (ISFOG II); 2010. p. 125–54.
[13] Plaxis. Plaxis 3D reference manual 2013 2013.
[14] Murff JD, Hamilton JM. P-ultimate for undrained analysis of laterally loaded piles. J Geotech. Eng 1993;119:91–107.
[15] Yu J, Huang M, Zhang C. Three-dimensional upper-bound analysis for ultimate bearing capacity of laterally loaded rigid pile in undrained clay. Can Geotech J 2015;52. http://dx.doi.org/10.1139/cgj-2014-0390.

[16] Zhang Y, Andersen KH, Tedesco G. Ultimate bearing capacity of laterally loaded piles in clay - some practical considerations. Mar Struct 2016;50:260–75.
[17] Baguelin F, Frank R, Said YH. Theoretical study of lateral reaction mechanism of piles. Geotechnique 1977;27:405–34.
[18] Bjerrum L. Problems of soil mechanics and construction on soft clays. Moscow. In: 8th international conference on soil mechanics and foundation engineering; 1973.
[19] Grimstad G, Andresen L, Jostad HP. NGI-ADP: anisotropic shear strength model for clay. Int J Numer Anal Methods Geomech 2012;36:483–97.
[20] Andersen KH. Cyclic soil parameters for offshore foundation design. In: Meyer V, editor. 3rd international symposium on frontiers in offshore geotechnics (ISFOG III). . Oslo, Norway: Taylor & Francis Group; 2015. p. 4–82.
[21] Lunne T, Long M, Forsberg CF. Characterisation and engineering properties of Onsøy clay. Singarpore: A.A. Balkema, Lisse, the Netherlands. In: Tan KKP TS, Hight DW, Cerark S, editors. International workshop on characterisation and engineering properties of natural soils, natural soils 2002; 2003. p. 395–428.
[22] Jeanjean P, Andersen KH, Kalsnes B. In: Soil parameters for design of suction caissons for Gulf of Mexico deepwater clays Offshore Technology Conference. Houston: Texas; 1998. p. OTC-8830-MS.
[23] Klar A, Osman AS. Predicting undrained displacement of piles under lateral loading. In: BM J, BM F, BA J, KJ A, editors. Second BGA international conference on foundations, ICOF2008. IHS BRE Press; 2008.
[24] Aubeny CP, Han S, Murff JD. Refined model for inclined load capacity of suction caissons. In: 22nd international conference on offshore mechanics and arctic engineering; 2003. Cancun, Mexico.
[25] Randolph MF. Analytical contributions to offshore geotechnical engineering. In: 18th international conference on soil mechanics and geotechnical engineering; 2013. p. 85–105. Paris, France.
[26] Vardanega PJ, Bolton MD. Strength mobilization in clays and silts. Can Geotech J 2011;48:1485–503.
[27] Vardanega PJ, Lau BH, Lam SY, Haigh SK, Madabhushi SPG, Bolton MD. Laboratory measurement of strength mobilisation in kaolin: link to stress history. Geotech Lett 2012;2:9–15.
[28] Abaqus. Abaqus 6.14–1 standard. Providence, RI, USA: Dassault Systèmes Simulia Corp.; 2014.